9. RESEARCH PROGRAM, ACCOMPLISHMENTS, AND PLANS

Period: March 15, 2007 to March 15, 2008

RESEARCH PROGRAM

Overview:

Our Center develops tools to study nanoscale systems.

For electronics and photonics, would like to synthesize new types of nanostructures, and visualize the motion of electrons and photons inside, using custom imaging techniques based on scanning probe microscopy.

For biology and medicine, we would like to understand how interacting cells behave as a system, and investigate the interior workings of cells, by developing powerful tools based on microfluidics and semiconductor technology.

Three Research Clusters address these goals:

Cluster I: Tools for Integrated Nanobiology builds bridges between the physical sciences, biology, and medicine. The physical sciences offer powerful new tools for manipulating and testing biological cells and tissues based on microfluidic systems, soft lithography, and semiconductor technology. In turn, biology and medicine offer an enormous range of engaging problems in functional biological systems, and the opportunity to think about "hybrid" systems that combine biological and non-biological components.

Cluster II: Nanoscale Building Blocks addresses the synthesis of new classes of nanostructures that exhibit size-dependent properties. An emphasis is placed on zero, one-and two-dimensional nanostructures, including nanoparticles, nanowires and heterostructures. Techniques to synthesize nanostructures from new materials are being developed, including oxide semiconductors and metal chalcogenides. These nanoscale building blocks provide new approaches for nanoelectronics and nanophotonics as well as sensors for biological systems.

Cluster III: Imaging at the Nanoscale explores new ways to image the quantum behavior of electrons and photons in nanostructures using custom-made scanning probe microscopes (SPMs). These instruments include cooled SPMs for the capacitive probing of electrons inside nanostructures, a cooled scanning tunneling microscope (STM), an STM equipped for Ballistic Electron Emission Microscopy (BEEM), and nearfield scanning optical microscopes (NSOMs). These tools are used to develop and understand the behavior of nanoelectronic and nanophotonic devices.

CLUSTER 1: Tools for Integrated Nanobiology

Coordinator: George M. Whitesides

Donhee Ham (SEAS, Harvard)	Howard A. Stone (SEAS, Harvard)
Efthimios Kaxiras (Physics & SEAS, Harvard)	Robert M. Westervelt (SEAS & Physics, Harvard)
	George M. Whitesides (Chemistry, Harvard)
Kevin (Kit) Parker (SEAS, Harvard)	Xiaowei Zhuang (Chemistry, Physics, Harvard)

***Collaborators*:** Rick Rogers (School of Public Health, Harvard) Giannoula Klement (Children's Hospital, Harvard), Ralph Weissleder (Medical School, Harvard), Mara G. Prentiss (Physics, Harvard), and X. Sunney Xie (Chemistry, Harvard)

Number of postdoctoral fellows: 4
Number of graduate students: 3
Number of undergraduate students: 3

Introduction

As biology begins to ask more quantitative and analytical questions about the nature of the cell, it needs new tools to study subcellular structures that have nanoscale dimensions. An important task is to build bridges between the physical and biological sciences. The physical sciences offer to biology new measurement tools and new procedures for analyzing the information obtained. In turn, biology offers to the physical sciences an enormous range of engaging problems, and stimulating examples of very sophisticated, functional biological systems. It also offers the opportunity to think about "hybrid" systems that combine biological and non-biological components.

The interface between the biological and physical sciences is one with enormous promise for fundamentally new science and, ultimately, technology. By supporting collaborations between investigators in the School of Engineering and Applied Sciences (SEAS), the Dept. of Chemistry and Chemical Biology, the Medical School, and the School of Public Health at Harvard, Cluster 1 will catalyze and expand a series of very effective collaborations across the physical-biological interface.

We expect three outcomes:

Tools for Cellular Biology and Tissue Culture: One of the major contributions that the physical sciences can offer to biology are new physical tools that can provide new kinds of information about cells and tissues.

The Science and Engineering of Interfaces between Animate and Inanimate Systems: This research will contribute to studies of cells in cell cultures, and to the assembly of groups of cells of the same or different types. In society, it will contribute to engineering the interface between patients and prostheses.

Tools for the Development of Drugs: The control over cells afforded by new microfluidic tools will be the basis for entirely new types of bioassay that will be important as the pharmaceutical industry moves away from information-poor animal

assays in preclinical studies toward more informative studies based on primary human cells.

Significant Achievements

In the past year, important new tools have been developed by research in this Cluster:

Donhee Ham, working with Ralph Weissleder's group at MGH, developed a miniaturized NMR relaxometry system that can be held in your hand. It consists of a small permanent magnet, a microcoil, and a custom-made RF transceiver integrated in a silicon chip. The goal is to make a portable NMR relaxometer that can detect biomolecules for diagnostic purposes. Weissleder's 'magnetic switch' technique uses activated magnetic beads as biosensors — on detection the beads clump, changing the T_2 relaxation time for water molecules nearby. This is the smallest complete compact NMR relaxometry system, more than an order of magnitude smaller, lighter and more sensitive than a commonly used commercial benchtop system. It will open the use this biosensing technique to a much wider use.

Kit Parker has developed an approach to nanoassembly of nanocomponents, such as those made in the *Nanoscale Building Blocks* Cluster, using AFM tips functionalized with antibody-doped polypyrole. He has shown that these tips bind with molecular selectivity to the objects tagged with the appropriate antigen. Furthermore, the binding can be turned on and off by reversing the sign of a voltage applied between the tip and the solution, so that the object can be released at the desired location. The process can be viewed by using an inverted optical microscope. Parker's technique provides an attractive way to visualize, pick up, and assemble very small objects in a fluid.

We have also advanced our understanding of biological systems:

Howard Stone has studied mechanically induced ATP release from red blood cells, to understand the pathways relevant to mechanical cell signaling. The goal was to understand how sudden modifications in shear stress could cause an increase in the ARP realease. He used a microfluidic system containing a narrow constriction to cause a sudden increase in the shear stress, and detected ATP release via a chemiluminescent reaction with luiferin/luciferase. Stone showed that flow through the constriction caused ATP release, and found this release was not a simple consequence of lysis.

Research in this cluster also developed a new approach to nanofabrication:

George Whitesides, working with Federico Capasso, created a simple way to fabricate arrays of metal and metal-oxide (ITO) nanotubes. Arrays of hollow tubes with heights up to 2 microns with diameters 20–200 nm, could be produced over cm^2 areas by evaporating the desired material onto anodized aluminum oxide. This technique was demonstrated with ITO, a transparent conductor, and with platinum, nickel and gold. The arrays have a high surface-to-area ratio, and they could be used as electrodes for three-dimensional solar cells and LEDs, as well as for electrochromic devices and batteries. Due to their large surface area, they could also be used as a template for depositing thin layers of molecules or polymers.

Simple Methods for Nanofabrication

George M. Whitesides
Chemistry, Harvard University
***Collaborator**:* Federico Capasso (Harvard)

Fabrication of Arrays of Metal and Metal-Oxide Nanotubes by Shadow Evaporation

The goal of our project was to develop a simple method to fabricate arrays of metal and metal-oxide nanotubes with controlled geometry. Dense arrays of uniform nanotubes are useful as electrodes for three-dimensional, nanostructured versions of devices such as solar cells, light-emitting diodes (LEDs), electrochromics, and batteries because they provide i) a high ratio of surface area to volume for interfacial charge collection/ separation, ion transport across liquid/solid interfaces (i.e., for mass-transport-limited processes in general), and ii) a template for depositing nanostructured films of small molecules or polymers that serve as optically and electronically active layers for these devices. We were particularly interested in fabricating arrays of indium tin oxide (ITO) tubes; there have been many efforts to fabricate nanostructures of ITO (the most popular transparent conducting oxide for use in such devices), but our work is the first to produce uniform, free-standing ordered arrays of electrically connected ITO nanotubes with controllable dimensions.

We developed a simple technique that involves depositing material onto an anodized aluminum oxide (AAO) membrane template using a collimated electron beam (e-beam) evaporation source. The evaporating material enters the porous openings of the AAO membrane and deposits on to the walls of the pores. The membrane is tilted with respect to the column of evaporating material, so the shadows cast by the openings of the pores onto the inside walls of the pores defines the geometry of the tubes. Rotation of the membrane during evaporation ensures uniform deposition inside the pores. Our work is the first to use e-beam evaporation—which is a highly collimated evaporation technique—to control the heights of the tubes. After evaporation, dissolution of the AAO in base easily removes the template to yield an array of nanotubes connected by a thin backing of the same metal or metal-oxide. The diameter of the pores dictates the diameter of the tubes, and the incident angle of evaporation determines the height of the tubes.

We fabricated arrays of tubes up to two μm in height, and 20–200 nm in diameter over large areas (~cm^2). Our method is adaptable to any material that can be vapor-deposited, including indium-tin oxide (ITO) (Fig. 1.1), a material that is useful for many opto-electronic applications. We also demonstrated the formation of arrays of nanotubes composed of platinum (a material useful for electrochemistry), nickel (a magnetic material), and gold. The array of gold nanotubes served as a substrate for surface-enhanced Raman spectroscopy (SERS): the Raman signal (per molecule) from a monolayer of benzenethiolate was a factor of ~5 x 10^5 greater than that obtained using bulk liquid benzenethiol. This work was done in collaboration with Prof. Capasso's group in SEAS, and was accepted for publication in ACS Nano.

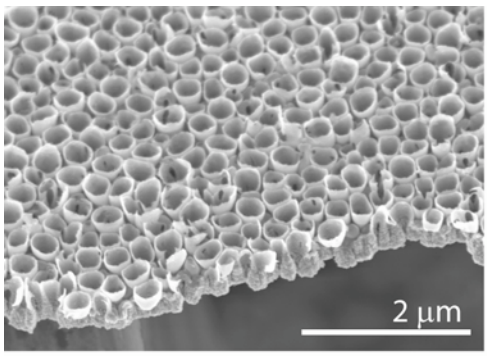

Figure 1.1. A SEM image of indium-tin oxide (ITO) nanostructures formed by line-of-sight evaporation into sacrificial anodized aluminum oxide pores. The heights and diameters of the tubes are ~ 200 nm.

Laterally Ordered Heterojunction of Conjugated Polymers: Nanoskiving a Jelly Roll

This project involves the fabrication of a nanostructured heterojunction of two conjugated polymers by a process comprising three steps: i) Spin-coating a multilayered film of the two polymers, ii) rolling the film into a cylinder (a "jelly roll"), and iii) sectioning the film with an ultramicrotome (nanoskiving). We used the photoactive, conjugated polymers poly(benzimidazobenzophenanthroline ladder) (BBL, n-type) and poly(2-methoxy-5-(2'-ethylhexyloxy)-1,4-phenylenevinylene) (MEH-PPV, p-type). The procedure produces sections with an interdigitated junction of the two polymers. The spacing between the materials within the section is determined by spin-coating (15–100 nm) and the height of each section is determined by the ultramicrotome (30 nm to 10 mm). The minimum thickness of the MEH-PPV layers accessible with this technique (~15 nm) is within the exciton diffusion length for the polymer (10–20 nm). We fabricated devices consisting of sections of the jelly rolls, BBL and MEH-PPV buffer layers, and electrodes. When exposed to white light from a halogen source, the sections produced a photovoltaic effect.

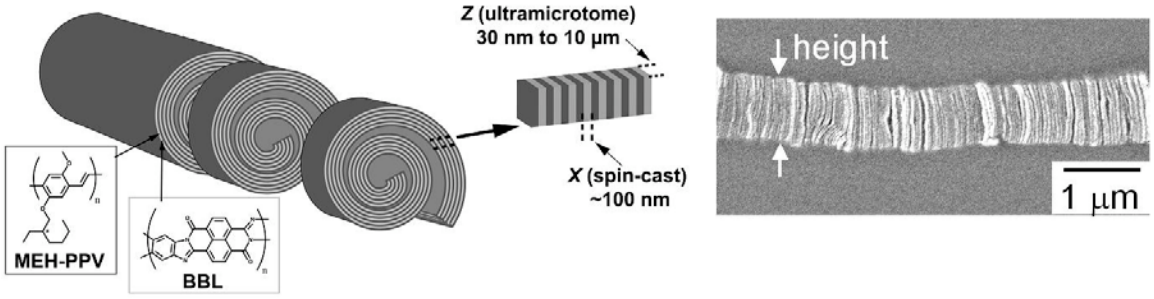

Figure 1.2. The figure shows a schematic drawing of the conjugated polymer jelly roll of MEH-PPV and BBL (chemical structures shown). The height of the sections is determined by the ultramicrotome and the width of the two materials within the sections is determined by spin-casting. The image is a scanning electron micrograph of the cross section of the heterojunction, that is, the orientation that the layers would have in a device.

Miniaturized NMR System

Donhee Ham

Electrical Engineering, Harvard University

Collaborator(s): Ralph Weissleder (Mass. General Hospital)

Research Goal, Approach and Accomplishments. In this work [*Cluster 1: Tools of Integrated Nanobiology*], Donhee Ham's group, in collaboration with Ralph Weissleder's group at MGH, sought to develop a miniaturized NMR relaxometry system, by using a small, fist-sized magnet and an in-housed fabricated microcoil together with an RF transceiver integrated in a silicon chip. The ultimate goal was to build a portable NMR relaxometer, which can detect biomolecules for diagnostic purposes. We carried out this work successfully, and constructed the smallest complete NMR relaxometry system, which is 40 times smaller, 60 times lighter, yet 60 times more sensitive than a commonly-used, state-of-the-art commercial benchtop system [1]. Figure 1.3 shows the photo of our mini NMR system. Its functionality was demonstrated through proton NMR measurements in water, and via biomolecular detection.

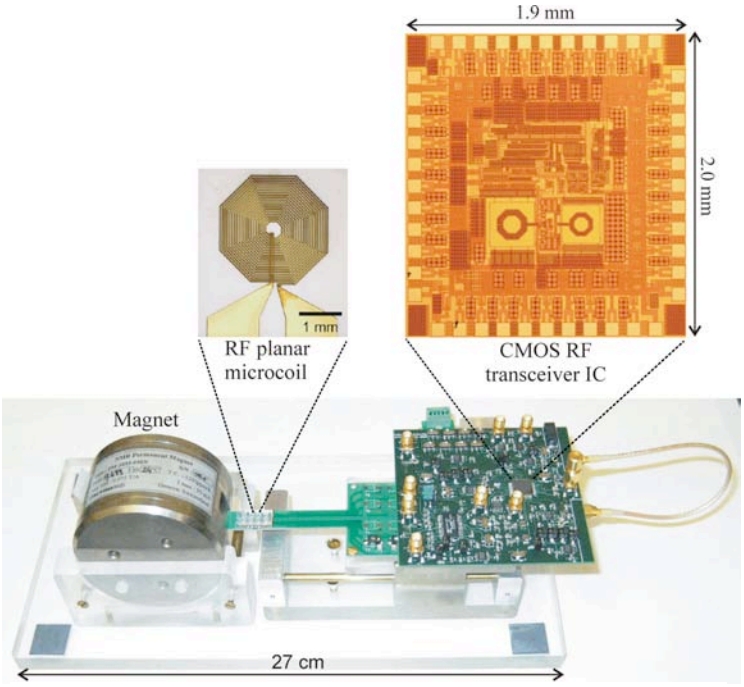

Figure 1.3. The CMOS mini NMR system [1].

The key challenge that we faced in this development was not just the integration of the RF transceiver, but to improve the performance of the integrated RF transceiver beyond what is typically required in larger NMR systems. This was because we had to overcome adverse conditions for NMR detection created by the low-quality magnetic field (weak strength of 0.5 T and pronounced inhomogeneity) of the small, low-cost magnet, which was necessary for the system miniaturization.

The RF transceiver we designed includes front-end low noise amplifiers (LNA), variable gain amplifiers (VGA), mixers, and pulse sequencers in a heterodyning configuration with lock-in amplification element. The receiver part of the transceiver achieved an overall input referred noise of only 2.5 $nV/Hz^{(1/2)}$, with which we were able to pick up NMR signals down to a few μV level. The transmitter portion of our transceiver was able to vary the power amplitude and pulse width in conjunction with a digital pulse sequencer, with which we were able to control the Rabi oscillation frequency with a proper pulse sequence to create the spin echo to overcome the

inhomogeniety of magnetic field for relaxometry. Figure 1.4 shows the RF transceiver architecture.

Figure 1.4 shows the detected spin echos where the NMR experiment was done with water protons. The top of Figure 1.4 is the spin echos when a smaller concentration of magnetic particles (0.1 mM) was put into the water. The bottom of the figure is the spin echos when a larger concentration of magnetic particles (1 mM) was put into the water. The magnetic particles spatially and temporally modulate spin precession frequencies, and hence accelerate spin-spin relaxation. The decreased spin-spin relaxation time T_2 with the increase of magnetic particle concentration is evident in Figure 1.4. Measured T_2 times with various particle concentrations match the theory.

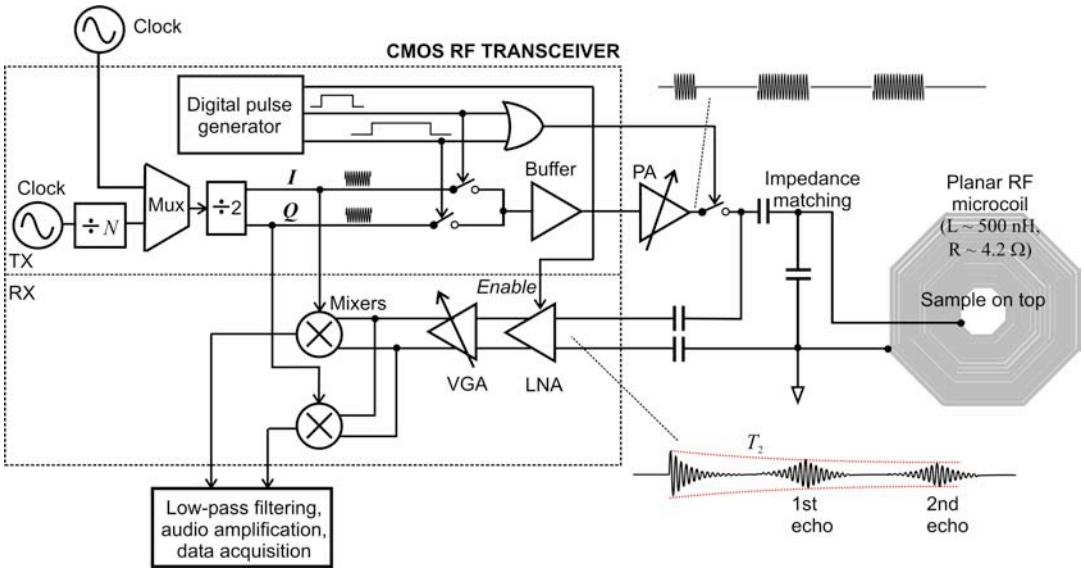

Figure 1.4. CMOS RF transceiver architecture used in the mini-NMR system.

Figure 1.5 shows the capability of our system as a biomolecular sensor. Magnetic nanoparticles coated with biotin that bind to avidin are put into a sample. If avidin exists in the sample (Fig. 1.5, *bottom*), the magnetic particles assemble into clusters [2]. These clusters reduce T_2, by accelerating the spin dephasing process. In the absence of avidin (Fig. 1.5, *top*), the magnetic particles remain mono-disperse in the sample, showing a smaller T_2 time in comparison to the case where avidin existed. The detection sensitivity for avidin is 20 fmol in mass, and 4 nM in concentration. The mass sensi-tivity is 60 times more than the commercial, state-of-the-art NMR relaxometry system. This detection sensitivity was limited by the assay, and our collaborator (Ralph Weissleder; MGH)'s newly developed assay can improve the detection level down to pM range. We also performed detection of folic acid, and are in currently the process of performing sensing experiments with various other biomolecules, including cancer marker proteins.

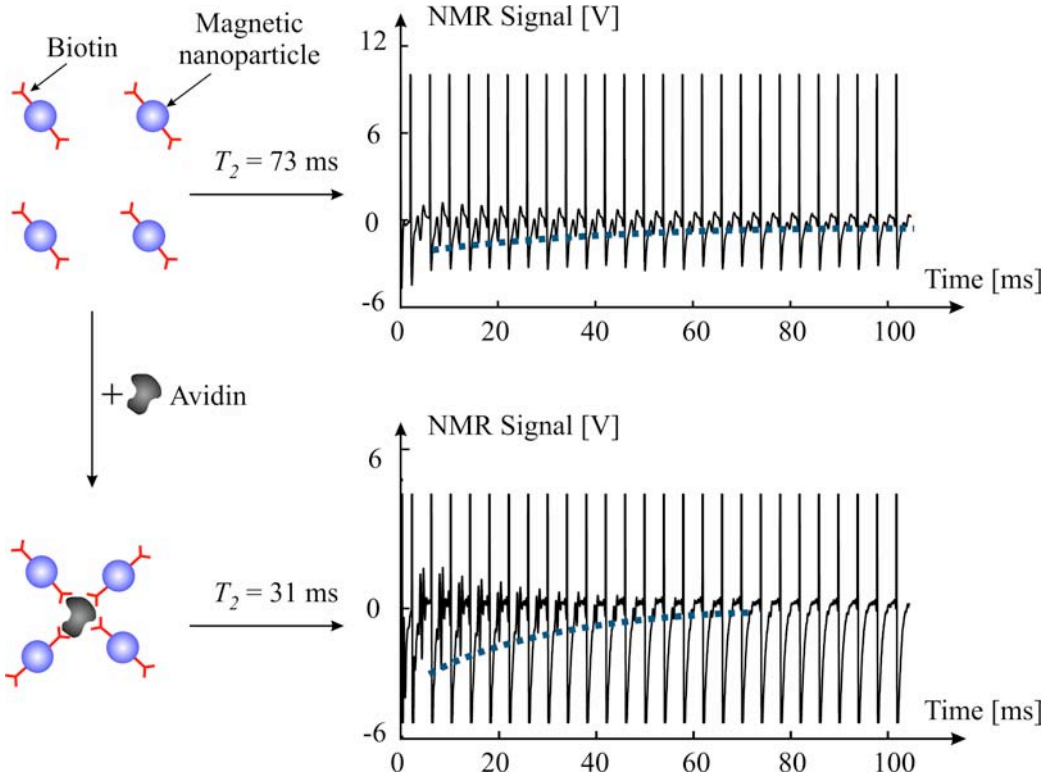

Figure 1.5. Experimental avidin detection using the CMOS mini-NMR system.

References

[1] Y. Liu, N. Sun, H. Lee, R. Weissleder, and D. Ham, *IEEE ISSCC*, pp. 140–141 (2008).
[2] J. M. Perez *et al*, *Nature Biotechnology* **20**, 816 (August 2002).

Molecular Robotics for Nanomanufacturing

Kevin (Kit) Parker
Bioengineering, Harvard University

Plan Using AFM tips functionalized with antibody-doped polypyrrole (Ppy) tips, we will use the entrapped proteins as actuators in building optical and electrical nanodevices. The first device that we will build is a 3-D array of fluorescent nanobeads by griping them

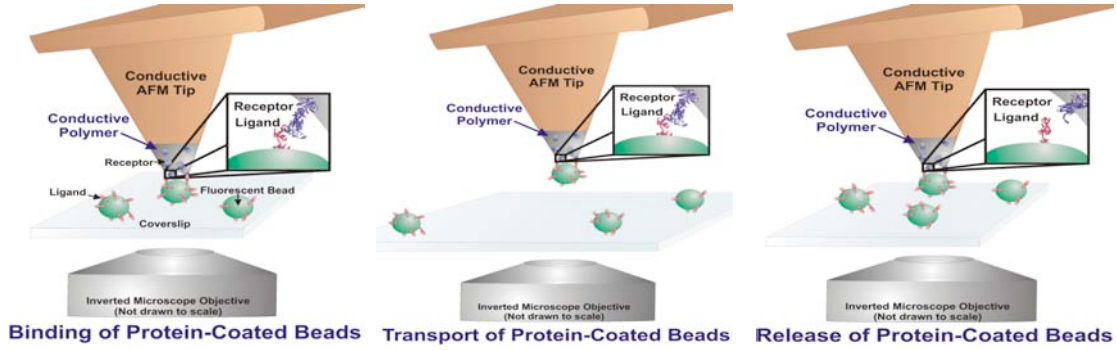

Figure 1.6. Experiment to demonstrate the ability to move protein-labeled cargo with the AFM tip.

with the instrumented AFM tip, moving them to the desired location, and releasing them from the tip (Fig. 1.6).

We will accomplish this in solution and during fluorescent video microscopy through an inverted optical microscopy coupled to a CCD camera. These experiments will allow us the ability to do real-time quality control assessments of our manufacturing technique and quantitative measurements of the speed of bead binding and release and the accuracy of their placement. An example image from a preliminary experiment is depicted in Fig. 1.7A. In this frame, we used a PPy instrumented AFM tip, doped with anti-FN, to bind micron scale fluorescent beads coated in FN. Upon binding, we moved them short distances for release. The red square in the image is a fidicual marker (microcontact printed red fluorescent protein) of known dimensions. These markers are important, because they allow us to do a quantitative comparison of bead placement versus the intended location, as programmed with the Igor programming language in our Asylum MFP-3D AFM. These experiments were conducted with microscale beads and flat AFM tips (Fig. 1.7B). Release kinetics and accurate repeatability were difficult to achieve with these tips.

In the proposed experiments, we will make instrumented, pointed AFM tips designed to bind FN-coated fluorescent beads and place them with greater accuracy than our initial, feasibility studies. In these experiments, we will attempt to build a nanoscale Christmas tree by alternate stacking of green and red fluorescent nanobeads. The structures will be structurally reinforced by protein-protein binding events facilitated by the FN coating on the green fluorescent bead and the a-FN coating on the red fluorescent beads. Stacking beads of alternating coating will require a pair of machined AFM tips,

each with its PPy tip doped with either a-FN (for picking up green beads) or FN (for picking up red beads). Beads can be kept in a well, or scattered on the substrate surface.

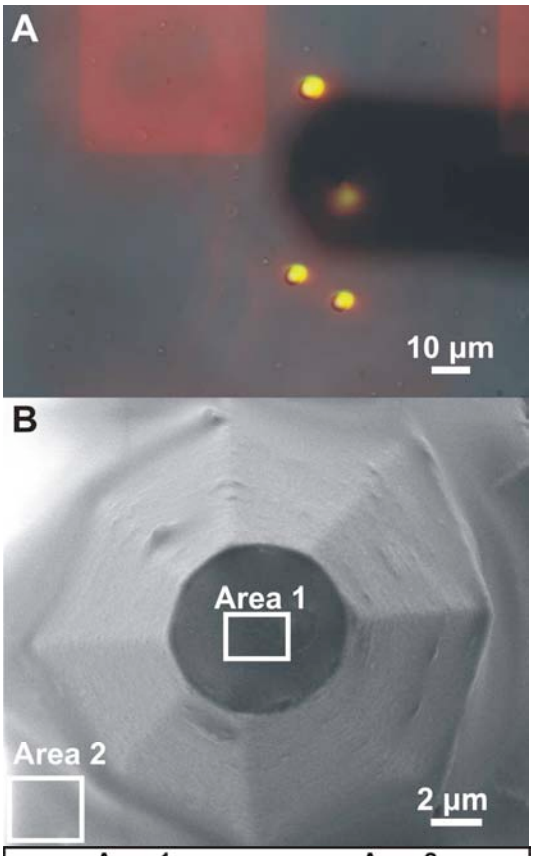

Area 1		Area 2	
Element	Atomic %	Element	Atomic %
Carbon	46.59 %	Silicon	100 %
Oxygen	26.69 %		
Gold	26.72 %		

Figure 1.7. **A**) PPy instrumented cantilever (shadow) moving 4 mm fluorescent beads (yellow). A ~40 mm square protein island (red) serves as a fidicual marker (red) during the experiments. **B**) Custom-built AFM cantilever with PPy tip. **Table**) Energy dispersive spectroscopy (EDS) of the tip demonstrates that PPy is deposited solely at the AFM tip (lower table, reference to B).

Microfluidic Study of ATP Release of Red Blood Cells

Howard A. Stone
Materials and Fluid Mechanics, Harvard University

We have undertaken a multi-direction study of mechanically induced ATP release from red blood cells. ATP is the standard energy currency for a cell and is a well-known signaling molecule. Therefore, it is important to better understand the various ways that red blood cells release ATP. Note that there remain controversies about the molecular-level details of how ATP is actually released from the cells, e.g., whether via a membrane channel or some other mechanism. We are (i) using microfluidic approaches to quantify under controlled conditions the ways in which sudden modifications of the (average) shear stress cause an increase in the rate of ATP release, and (ii) examining how electric fields, applied in pulses, cause changes in ATP release. The two studies, taken together, will add quantitative and qualitative insights into an important though incompletely characterized pathways relevant to mechanically induced cell signaling. The approach may we have taken also be potentially useful down the road for studying how other signalling molecules are released in response to stresses.

Microfluidic Approaches for Controlled Studies of ATP Release due to Mechanical (Shear) Stress

The basic experimental setup used to deform erythrocytes and detect ATP via a chemiluminescent reaction with luciferin/ luciferase is shown in Figure 1.8. The width of the central (deformation) channel varies from 20–50 μm to quantitatively observe the shear stress effect; we also vary the length of the central (deformation) channel from 70–3200 μm to observe the cell response-kinetics at constant shear stress. The height of the channels are all the same (38 μm). The kinetic data are collected by changing the position (X) of the objectives; because of the low light levels, a photomultiplier tube is used to monitor that light levels which are related to the rate of ATP release. The average shear stress is changed either by changing the average flow speed or by having a step change in the channel width. Changing the channel length also increases the duration of the application of the higher shear stress.

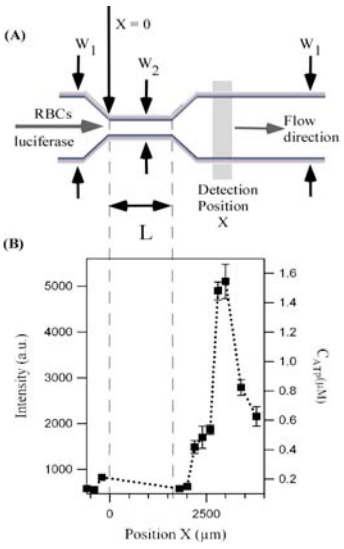

Figure 1.8. (**A**) Microfluidic experiment for changing the magniutude and duration of the average shear stress. (**B**) Measurement of the light intensity at different positions along the channel.

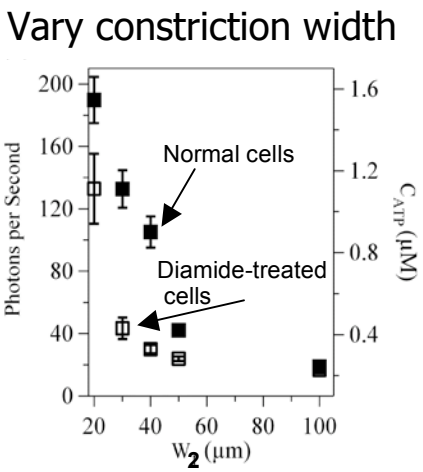

Figure 1.9. The effect of changing the width of the constriction on the measured ATP release. Also, changing the rigidity of the cell by adding diamide has a significant influence on the results.

Typical results are shown in Figure 1.9, which illustrates (a) that increased shear stress (narrower channels) increases the ATP release, and (b) making the cell more rigid (by treatment with diamide) can inhibit ATP release even when the shear stress is enhanced, which also indicates that the results are not a simple consequence of cell lysis.

Furthermore, as the channel length is changed, we have observed systematic changes in the ATP release. This may either be due to the increased time over which the shear stress is applied or may give some insights in to the kinetics of the biochemical pathway responsible for triggering the mechanosensing response.

We are pursuing these and related experiments in order to better understand these new results. There is only a little work that we know of using the controlled conditions from microfluidics in order to probe the nanoscale physics and chemistry responsible for ATP release under stress.

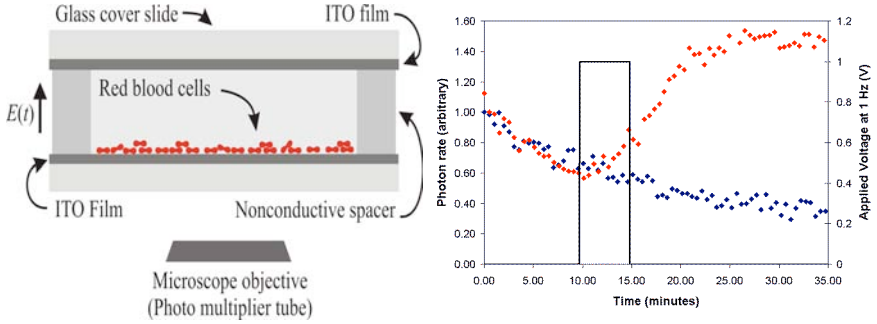

Figure 1.10. Experiments for studying the influence of electric fields on ATP release from red blood cells.

Electric Field Effects on ATP Release from Red Blood Cells

We have observed that electric fields have systematic effects on ATP release from red blood cells. Again, we are observing the ATP release using the well-known bioluminescent reaction.

The experimental setup is shown in Figure 1.10 (*Left*). A suspension of RBCs rests on an ITO electrode. An oscillatory field (typically 1 V, 1 Hz) is applied, and light emitted by the reaction between ATP and luciferase is measured with a photo-multiplier tube. Typical response curves are shown on the right. In the absence of an applied field (blue points), the rate of photon emission decays with time as extracellular ATP is consumed. Application of an electric field (red points) induces a rapid increase in extracellular ATP.

We have visual observations that suggest these results are not simply due to cell lysis. In addition, the fields we use are typically significantly lower than those required for cell lysis. We are continuing these experiments, which we believe are new directions in the study of ATP release from cells.

Size Segregation of Giant Unilamellar Vesicles

We have discovered an electric field mediated route to separate giant unilamellar vesicles (tens to hundreds of microns in diameter) from a suspension of vesicles made by electro-formation that typically have diameters from nanometers to microns (with the majority in the submicron range). The experiment is shown in Figure 1.11.

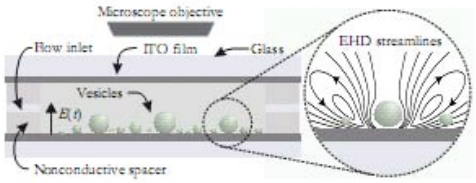

Figure 1.11. Experimental apparatus for electrohydrodynamic stratification of vesicles with small vesicles adjacent to the boundary and larger vesicles typically resting on the smaller vesicles.

We then use a sequence of an electric pulse, which causes small vesicles adjacent to the electrode to stick, and a gentle flow in the microfluidic channel which advects the larger vesicles (Fig. 1,12). The separation efficiency is high with more than 90% of the larger vesicles being removed.

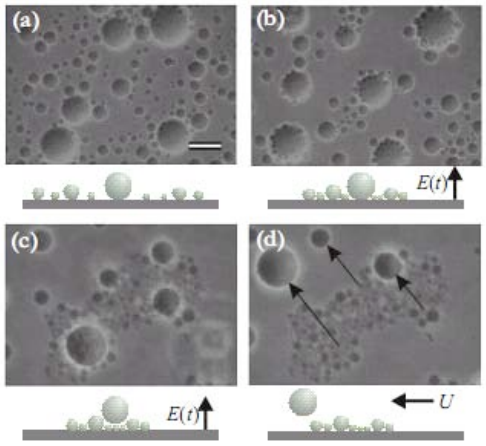

Figure 1.12. Main stages of the EHD size separation process. (**a**) Prior to application of the field, the vesicles are arranged randomly near the electrode. (**b**) 30 seconds after application of a 10 V, 30 Hz AC field, smaller vesicles have aggregated around larger ones. (**c**) After 10 minutes of continuous application of the electric field, most of the larger vesicles have been lifted on top of clusters of smaller vesicles. (**d**) After a short DC pulse adheres the smaller vesicles to the electrode, a gentle pressure-driven flow (in direction of arrows) removes the larger vesicles. Scale bar in (a) is 25 μm.

Fluorescent Metal Nanoparticles for Bioimaging

Xiaowei Zhuang
Chemistry, Physics, Harvard University
Collaborator: Z.L. Wang (Georgia Tech)

Imaging individual biomolecules and their dynamics in living cells provides new opportunities to advance our understanding of biological systems. A major challenge in bioimaging is the detection of small molecules such as metabolites, signaling and drug molecules, which play central roles in many cellular functions. Noble metals exhibit versatile optical properties at the nanometer scales, and thus may function as novel imaging probes and sensors. In particular, the strong Raman enhancements from noble metal nanostructures facilitate imaging of fingerprint vibrational spectra of small molecules, offering a new strategy for detecting small molecules.

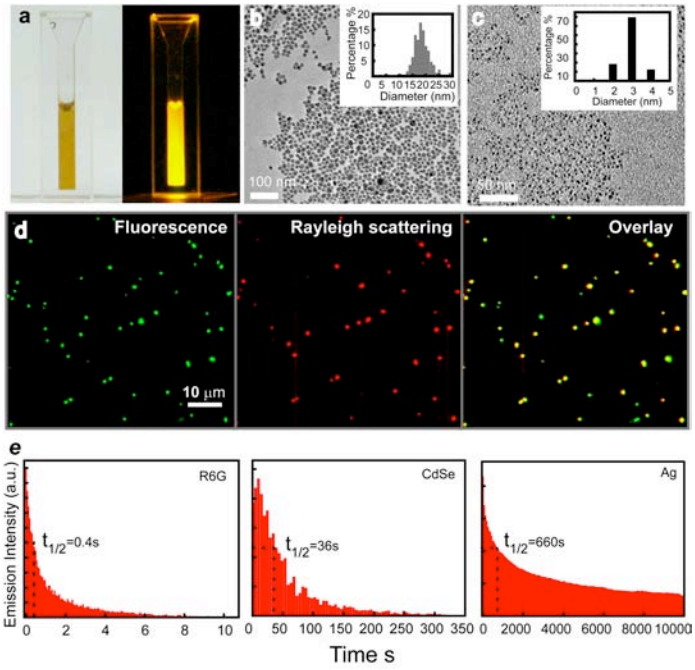

Figure 1.13. Fluorescent and Raman active silver nanoparticles**.** (**a**) Photos of an aqueous solution of fluorescent silver nanoparticles created by thermal reduction in a glycine matrix. The pictures were taken without (left) and with (right) 532 nm laser excitation. TEM images and size distribution of purified silver nanoparticles of ~20 nm (**b**) and ~3 nm (**c**). (**d**) Fluorescence, Rayleigh scattering and overlay images of the silver nanoparticles created by solid-phase synthesis, indicating that more than 95% percent of particles are fluorescent. (**e**) Comparison of photostability of R6G, quantum dots and silver nanoparticles. Shown here is the total intensity of fluorescenc emission from many particles/molecules as a funciton of time, indicating that the silver nanoparticles are much more stable compared to quantum dots and dyme molecules

As a part of the Cluster 1 — Tools for Integrated Nanobiology, we developed silver nanoparticle based indicators that hold great promise for imaging cellular dynamics of biomolecules and their chemical environment *in vivo*. During the last funding period, we discovered a simple solid-phase thermolysis method that can readily produce fluorescent and Raman active silver nanoparticles with diameters tunable from 2 to 20 nm (Fig. 1.13 a-c). Single purification methods such as centrifugation allows mono-dispersed nanoparticles to be isolated. Comparison of the Rayleigh scattering (dark field) and fluorescence images revealed that more than 95% of the nanoparticles were fluorescent (Fig. 1.13 d). This was in contrast to colloidal silver nanoparticles prepared by typical solution phase methods, where only ~2% of the particles emit fluorescence. Emission from these nanoparticles was remarkably bright and photostable: the average total number of photons emitted individual silver nanoparticles before photobleaching is 7 x 10^{10}, 2 orders of magnitude

greater than that from individual quantum dots (CdSe/ZnS core-shell quantum dots, λ_{max} = 605 nm) and 5 orders of magnitude larger than that from single dye molecules (Rhodamine 6G).

The detailed structures of these fluorescent and Raman-active silver nanoparticles were characterized using high resolution transmission electron microscopy and photo-electron spectroscopy in Center of Nanosystems at Harvard and in our collaborator Z.L. Wang's lab at Georgia Tech. These nanoparticles exhibit a multicrystal structure with domain sizes down to 1 nm or less, revealing crucial roles of grain size and crystallinity in optical properties of metal nanoparticles (Figs. 1.14 a-c).

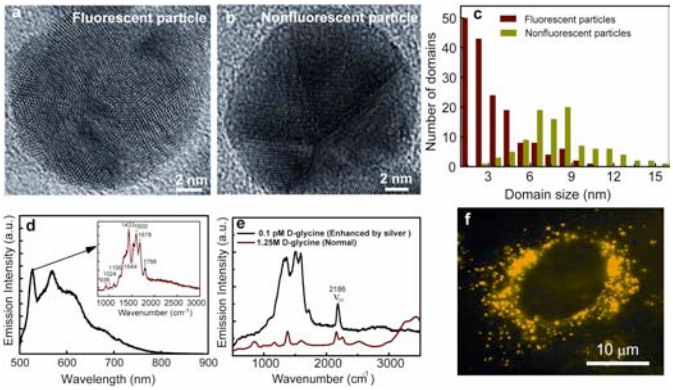

Figure 1.14. Structure characterization and spectroscopic properties of fluorescent silver nanoparticles**.** (**a,b**) TEM images of a fluorescent nanoparticle created by our solid-phase synthesis method and a nonfluorescent nanoparticle created by solution-phase synthesis. (**c**) Domain size distributions of the fluorescent (red) and nonfluorescent (green) nanoparticles. (**d**) Single-particle emission spectra of a fluorescent nanoparticle. **Inset:** The Raman peak was further resolved into multiple lines that correspond to various vibrational modes of the glycine coat on the particle. (**e**) Enhanced Raman spectrum of 0.1 pM D-glycine detected near a silver nanoparticle (black line) in comparison with the normal Raman spectrum of 1.25 M glycine without silver nanopartile enhancement (red line). Peak at 2186 cm^{-1} corresponds to the C-D vibrational line. (**f**) Fluorescence image of a live cell labeled with silver nanoparticles.

The bulk emission spectrum of the nanoparticles revealed a sharp Raman peak at the short wavelength end superimposed on a broad fluorescence band (Fig. 1.14 d, black line). The Raman peak can be further resolved into multiple lines, which arise from the glycine molecules on the surface of silver nanoparticles. We further quantified the Raman enhancement effect and explore the sensing power of these silver nanoparticles by immersing these silver particles in low concentrations of deuterated glycine (D-glycine) solution. A pronounced Raman line at 2186 cm^{-1} was observed from single silver nanoparticles, which arises from C-D vibration of D-glycine (Fig. 1.14 e). By comparing the signal strength of enhanced C-D Raman scattering from a single D-glycine molecule with that of normal Raman scattering from D-glycine solution of 1.25 M, we found that the Raman enhancement factor from a single fluorescent silver nanoparticle was on the order of 10^{14}. Preliminary studies on the bioimaging application of these silver nanoparticles indicated that these silver nanoparticles were also compatible with cell imaging – fluorescence from the particles attached to a live cell was not quenched but showed similar intensity as measured in water (Fig. 1.14 f).

To explore bioimaging applications of these nanoparticles we plan to accomplish the following aims in the next year.

I. Create Raman reporters for simultaneous imaging of different biomolecules. Giant Raman enhancements from fluorescent silver nanoparticles allow visualization of vibrational fingerprints of ligand molecules on the particle surface. We can take

advantage of this unique property to create silver nanoparticles with distinctive Raman signatures by coating the particles with different small molecules. Thus, a variety of biomolecules can be labeled by the fluorescent silver nanoparticles and also can be distinguished based on different Raman signatures of the particles.

II. Develop bioconjugation chemistry for specific labeling of biomolecules and study their localization and transport properties in live cells. One strategy is to use dual functional polyethylene glycol, which can protect silver nanoparticles and also serve as a linker for antibody or other biomolecule conjugation.

III. Imaging small molecules in live cells using these nanoparticle indicators.

IV. Create dual functional probes for bioimaging and gene delivery. We recently created glutathione coated fluorescent gold nanoparticles of ~2 nm and found that these gold nanoparticles can quickly enter nuclei of live cells and bind to chromosomes. We will explore bioconjugation chemistry to functionalize these nanoparticles, so that they can selectively bind genome sequences of interest. In addition, we will also utilize the specific cellular pathways of these small gold nanoparticles to explore their potential in gene delivery.

Multiscale Modeling of DNA Translocation through Nanopores

Efthimios Kaxiras
Physics and Applied Physics, Harvard University
Collaborators:

Research Goal, Approach and Accomplishments. The capability of probing biophysical systems at the atomistic (nanometer) scale has opened exciting possibilities for understanding how nature has solved key problems working with atoms and molecules, while these systems also offer challenges for imitation. Our goal is to explore the structure and properties of nano-scale biophysical systems in order to develop a fundamental understanding of their nature and to suggest possible new applications. In response to this challenge, various strategies have been developed, which are in general referred to as multiscale modeling. In this project we have used multiscale approaches to simulate biological systems and investigate their physical properties. These computational schemes involve either concurrent or sequential coupling of the spatial and temporal scales involved in the dynamical evolution of complex biological systems.

I. Multi-fold Translocation of Biopolymers through Nanopores — Quantized Current Blockades

We have recently developed a multiscale framework [1] that involves different levels of the statistical description of matter (continuum and atomistic) through the spatial and temporal coupling of a *mesoscopic* fluid solvent, based on the lattice Boltzmann method, to the atomistic scale which employs explicit molecular dynamics. Our *multiscale* model has already proven efficient in describing biophysical processes, like the biopolymer translocation through nanopores. We have also been motivated to study such processes by recent experiments on DNA translocation through a nanopore [2,3], which aim to open a way for ultrafast DNA-sequencing by reading the base sequence as an electronic signal while the biopolymer passes through a nanopore. Experimentally, translocation is observed *in vitro* by pulling DNA molecules through micro-fabricated solid state or membrane channels under the effect of a localized electric field [2,3] through which a force is applied at the pore region that pulls the molecule through the pore in the presence of a fluid solvent.

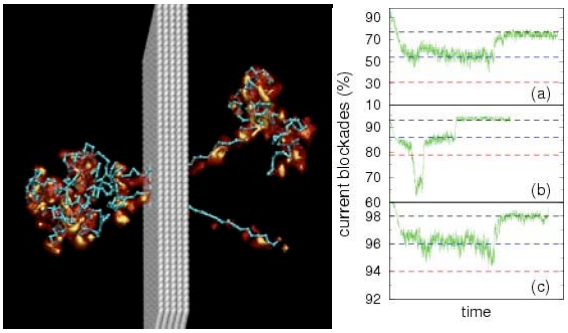

Figure 1.15. Left panel: 3-D visualization of the translocation process through a nanopore: The molecule as it passes through the pore is shown in cyan beads, together with the fluid velocity mapped on 3-D contours in the vicinity of the beads. Right panel: Current blockades with time for a (**a**) small, (**b**) mid-sized and (**c**) large pore diameter. Red, blue and black lines correspond to the blockade for a 3-fold, 2-fold and unfolded biopolymer conformation as this passes through the pore.

We performed a series of simulations for different initial realizations of the biopolymer, as well as various biopolymer lengths and pore sizes. The picture that emerges from our simulations provides evidence for quantized ion-current blockades depending on the folding configuration and offer detailed information on the role of hydrodynamic correlations in speeding-up the translocation process. We paid special attention to the morphological aspects of the translocation dynamics, i.e., the folding behavior (single versus multi-file configuration) of the translocating molecule as it goes through the pore, and the associated synergistic coupling (aiding of the molecular translocation by the surrounding solvent). We have reported the first computational evidence of quantized ion-current blockades, in good agreement with recent experimental observations [4], thus providing a *direct* independent confirmation of a close connection between the drop of voltage-bias across the nanopore and the underlying morphology of the translocating molecule. The acceleration due to this synergy is interpreted as the outcome of a renormalization of the actual pore geometry into an effective one, more conducive to translocation. This opens up exciting prospects for the development of optimized nano-hydrodynamic devices, like multi-translocation chips, based on the fine-tuning of hydrodynamic correlations. The present simulation technique offers an ideal complement to experimental studies aimed at developing innovative techniques for the study of molecular structures and the sequencing of their genetic content.

II. Modeling the Conformational Variability of DNA — Coarse Grain Potential for DNA Nucleotides

The conformational variability of DNA remains a problem of significant importance, especially in view of recent experimental studies of DNA translocation through solid nanopores and the DNA interaction with other nanostructures such as carbon nanotubes. In order to provide a realistic description of complex biological systems and efficiently simulate them, a coarse-grained model of DNA is desirable. Toward this goal, we derived effective coarse-grained interactions between DNA nucleotides from accurate density-functional-theory [4] calculations on DNA bases and base-pairs in various arrangements. The energy for hydrogen bonding E_{hb} is calculated as a function of the lateral distance between the DNA bases, and the stacking energy E_{st} between two base-pairs is calculated as a function of the twisting angle and vertical separation. The contribution to the energy from the sugar backbone E_{bb} is also taken into account. The results are fitted by simple analytical expressions. The parameters that enter in these expressions show a large sequence-dependent variability. The equation that describes the coarse grain potential is:

$$U_{tot} = \sum_{b} E_{hb}(x_{hb}) + 2E_{bb}(z_{st}) + \frac{1}{2}\sum_{bp} \frac{E_{tw}(\theta)}{E_{tw}(36^{o})} E_{st}(z_{ax})$$

where, x_{bb}, z_{st}, θ, z_{ax} are the characteristic lengths and angles shown in Figure 1.16, which define the positions and orientations of the bases and base-pairs.

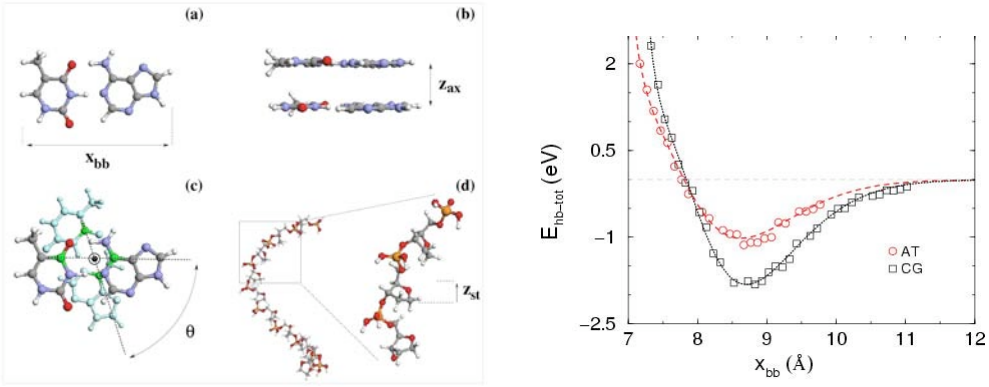

Figure 1.16. Atomistic representations of all the conformations considered in our calculations. (**a**) An AT base-pair separated at a distance x_{bb}, (**b**) two stacked AT-AT base-pairs (side view) at a separation z_{ax} along the DNA axis, (**c**) top view of two AT-AT base-pairs at a relative orientation θ with respect to the DNA axis (denoted by the dot) and (*d*) part of the sugar backbone; in the magnification the stretching variable z_{st} along the DNA axis is defined as the movement of one sugar site due to stretching. In the rightmost panel, as a representative of the energetic contributions within DNA, the hydrogen bonding potential for AT and CG base-pairs is shown with their horizontal separation x_{bb}. Both simulation data and the fitting curve (solid and dotted lines) are shown.

The construction of such an effective coarse grain potential for DNA nucleotides opens up the possibility of large-scale simulations of DNA, bridging the scales between the atomistic and the macroscopic. Modeling DNA molecules of length in the range of thousands of base-pairs will provide insight into the effects of the DNA sequence on its various transformations. Handling DNA lengths comparable to gene sizes, can also provide information about their interactions with histones and identify patterns in gene regulation. Work toward this goal is currently in progress.

References

1. M.G. Fyta, S. Melchionna, E. Kaxiras, and S. Succi, "Multiscale Modeling and Simulation," 5, 1156 (2006)
2. A.J. Storm *et al*., *Nanolett.* **5**, 1193 (2005).
3. J. Li ., *Nat. Mater*. **2**, 611 (2003).
4. P. Hohenberg and W. Kohn, *Phys. Rev*. **136,** B864 (1964); W. Kohn and L.J. Sham, *ibid*, 140 A1133 (1965); J.P. Perdew and A. Zunger, *Phys. Rev*. **B 23**, 5048 (1981).